Combinatorial tumor suppressor gene targeting immortalizes primary pancreatic ductal cells, resulting in temporal, deterministic structural patterns across the genome

Matthäus Felsenstein

matthaeus.felsenstein@charite.de

Charité – Universitätsmedizin Berlin

Mengwen Hu
Dou Ma
Jenny Tamboli
Cao Zhong Jing Jin
Ruonan Wang
Luan Xiao Hui
Frank Dubois
https://orcid.org/0000-0002-7654-6208
Christopher Neumann
Anna Dolnik
Karl Herbert Hillebrandt
Luna Haderer
Madalina Giurgiu
Anton Henssen
Kirsten Kübler
Johann Pratschke
Thomas Malinka
Igor Sauer
Laura Wood
Johns Hopkins University https://orcid.org/0000-0003-3096-652X
Nicholas Roberts
Johns Hopkins University https://orcid.org/0000-0002-8709-0664

Article

Keywords: Pancreatic precursor lesion, CRISPR gene targeting, Deterministic structural pattern

Posted Date: March 27th, 2026

DOI: https://doi.org/10.21203/rs.3.rs-9124723/v1

Additional Declarations: There is **NO** conflict of interest to disclose.

Abstract

Pancreatic carcinoma develops from pre-cancerous lesions. Limited sensitivity of current imaging modalities and biomarkers challenges early detection. Findings from murine in vivo models revealed deterministic structural patterns following heterozygous TP53 alteration. Few pancreatic duct cell culture models exist to study such molecular concepts in the early stages of the disease process. A Golden Gate assembly cloning method was used to generate multiplexed vectors that targeted the main pancreatic carcinoma driver genes (KRAS, CDKN2A, TP53, SMAD4). Their transient transfection was implemented in six experimental arms in HEK293T and primary ductal cells. Immortalized cell lines were characterized via established in vitro assays. In-depth whole exome (>30x) and nanopore sequencing (>15x) at two distinct evolutionary time points was conducted. Multiplexed vectors targeted main driver genes with an observed NHEJ (non-homologous end joining) efficiency of up to 25%. Following transient transfection of primary pancreatic ductal cells, six cell lines were generated from three patient samples, all of which exhibited loss of function in the two genes, CDKN2A and TP53. The immortalized cell lines maintained a duct cell phenotype. In-depth genomic signature analysis confirmed gene editing and revealed deterministic structural changes from early to later passages. Our study successfully demonstrated the immortalization of pancreatic duct epithelial cells through combinatorial CRISPR/Cas9 gene editing. The methodology could be expanded to other difficult-to-transfect cells. Driver gene targeting in human pancreatic ductal cells resulted in deterministic structural patterns that could explain the accelerated carcinogenesis at early stages.

Introduction

Pancreatic ductal adenocarcinoma is a highly aggressive and lethal malignancy. Despite accumulated knowledge regarding the molecular trajectory of the disease, widespread diagnostic tools for early detection or targeted therapies remains a necessity. Two phenotypically distinct molecular pathways lead to the development of pancreatic carcinoma.[1,2] The classic pathway is embodied by microscopic pancreatic intraepithelial neoplasia (PanIN) with accumulation of a small number of driver gene alterations (*KRAS, CDKN2A, TP53, SMAD4*) from low-grade to high-grade and invasive carcinoma.[3] The cystic precursor pathway, that elicits the development of intraductal papillary mucinous neoplasm (IPMN) or mucinous cyst neoplasm (MCN), regularly harbors *GNAS* and/or *RNF43* in addition to the classic driver gene alterations. While cystic precursors provide opportunities for earlier detection using state-of-the-art imaging modalities (CT, MRI), microscopic PanINs remain undetectable, and the invasive clones dislodge early into the surrounding ductal-, lymphatic- or venous vessel network.[4,5] The precise molecular signatures responsible for the transition from precursor to invasive carcinoma remain poorly understood. The recent in-depth study on PanIN biology from *Braxton AM et al*. using three-dimensional reconstruction of molecular signatures, highlighted the tremendous genetic heterogeneity and multifocality at earliest stages.[6] Identifying reliable biomarkers for the early detection of “at-risk” precursor lesions in liquid biopsy samples (e.g. pancreatic juice, plasma) prior the emergence of invasive or metastatic clones will require additional data from molecular models and human genomic analyses.

Genetically modified animal models (e.g. KC, KPC, other derivative GEMMs) have highlighted the role of acinar-duct metaplasia (ADM) in the pathogenesis of invasive carcinoma.[7,8] In brief, oncogenic $KRAS^{G12D}TP53^{hetMut}$ PDX^{+} progenitor cells rapidly develop multifocal PanIN lesions that can progress to invasive carcinoma and metastatic disease.[9,10] Recent data implies, that the development of pancreatic carcinoma is associated with deterministic genomic patterns following heterozygous p53 inactivation.[11] Early deleterious events in the diploid genome including loss of heterozygosity of $TP53^{R172H}$ with subsequent allelic imbalances and polyploidization, result in increased oncogenic $KRAS^{mut}$ and Myc^{mut} dosages, that provoke an aggressive phenotype with a high incidence of metastases.[12,13] Collectively, lineage tracing data in murine models yielded data on complex chromosomal alterations that result in accelerated disease progression. However, these observations require confirmation in human cells as well.

Versatile *in vitro* resources for modelling early, pre-malignant human disease stages are scarce. Besides HPNE, that seems to represent a unique intermediary cell line with mesenchymal features, the $HPDE^{E6E7}$ cells represent the only commercially available normal ductal cell culture model.[14] Exogenous $KRAS^{mut}$ expression in $HPDE^{E6E7}$ resulted in development of carcinoma *in vivo*, calling its accurate representation of healthy ductal cells into question.[15] Better understanding of required stem-cell factors has allowed reproducible three-dimensional human progenitor cell cultures to be derived from the exocrine lineage but this approach remains costly and laborious.[16,17] Precursor cell cultures directly derived from pre-malignant cystic lesions have complex genomic aberrations, likely through a selection of highly proliferative and aggressive clones.[18,19] Lately, three-dimensional cell cultures in a selected niche factor environment could elegantly demonstrate programmed enrichment of targeted genotypes.[20] Although the combination of these biotechnological advances (CRISPR/Cas9, pluripotent stem cells, organoid culture) brought the derivation and sustained culture of precursor cell types to the next level, no high-throughput resource for modelling the disease process of precursor towards invasion were derived at this point.

Previous work demonstrated that targeting established tumor suppressor genes in primary prostate epithelial cells resulted in immortalization of difficult-to-transfect epithelial cells despite normal karyotype and regular expression of the p53/pRB.[21,22] However, other multiplexed concepts have emerged that have induced carcinoma development based on combinatorial driver gene targeting in KC mice.[23] Using the Golden Gate assembly method, we developed multiplexed vectors to target the aforementioned critical driver genes for pancreatic carcinogenesis. Transient transfection resulted in the immortalization of non-transformed pancreatic duct epithelial cells, yielding genetically defined and primarily diploid *in vitro* precursor cell lines at initial passages. Such precursor cell models will be a critical resource for understanding early clonal and deterministic concepts in tumor evolution during pancreatic carcinogenesis.

Methods

Culture of cell lines and primary cells:The human PDAC (PANC-1 | RRID:CVCL_0480, AsPC-1 | RRID:CVCL_0152) and other carcinoma cell lines (HEK293T; CVCL_0063) were cultured at 37°C , with 5% carbon dioxide and 95% relative humidity in complete growth culture media recommended by ATCC (high-glucose DMEM/RPMI complete medium). The $HPDE^{E6E7}$ cell line (CVCL_4376) was obtained from commercial source (Tsao laboratory, Kerafast) and cultivated in keratinocyte medium supplemented with EGF and BPE (Thermo Fisher Scientific). The number of passages did not exceed P30. With ethical consent (EA4/108/19) from the institutional review bord, primary duct tissues were collected from pathologically confirmed, tumor free resection margins at surgical pathology. For culture, half of the freshly dissected pancreatic duct tissue was washed in HBSS at 4°C, minced and subsequently incubated with digestion solution (12.5mg collagenase IV, 2.5mg dispase in 5ml DMEM-high glucose complete medium). Other half, was used for downstream genomic analyses and germline screening for single nucleotide polymorphisms (SNP) or single nucleotide variants (SNVs). Following 60min incubation, the cell mixture was centrifuged and diluted in DMEM-high glucose complete growth medium. The cell suspension was uniformly distributed into 6-12 wells of 24-well plate, pre-coated with Collagen I from rat tail (Thermo Fisher Scientific). After five days of continuous culture in the cell culture incubator, cobblestone-like ductal epithelial cells were observed and the culture medium was then replaced with SFM-Keratinocyte Medium supplemented with EGF/BPE. The cells were permitted to proliferate under these conditions until they were to be utilized further or discarded in instances of fibroblast overgrowth (> 50% of total area).

Three-dimensional tissue culture: Human PDAC (PANC-1, AsPC-1) and primary duct cell lines (PD47, PD51, PD62) were dissociated and counted. A total of 2-5x10^5 cells per well (in 50µl) were submerged in liquified Matrigel and domes generated at the bottom of the well. Solidified domes were cultured in pancreas expansion media as previously described.[24] Cell clusters were sub-cultured every 3-4d. For enrichment of *TP53* mutant clones, tumoroids were cultured in pancreas expansion media supplemented with Nutlin-3a (5µM, Cayman chemical). For enrichment of *SMAD4* mutant clones, modified pancreas expansion media via removal of the Noggin supplement was generated.

Molecular cloning: Suitable guide RNAs (gRNA) for target genes (*KRAS, CDKN2A, TP53, SMAD4*) were designed using ChopChop and UCSC platform following recent recommendations.[25] Two possible high-performance nucleotide sequences (for in-situ generation of gRNAs) were generated for each target gene: KRAS gRNA1: GTAGTTGGAGCTGGTGGCGTAGG | KRAS gRNA2: CTGAATTAGCTGTATCGTCAAGG; CDKN2A gRNA1: GTGCACGGGTCGGGTGAGAGTGG | CDKN2A gRNA2: GGTACCGTGCGACATCGCGATGG; TP53 gRNA1: GCATGGGCGGCATGAACCGGAGG | TP53 gRNA2: GGTGCCCTATGAGCCGCCTGAGG; SMAD4 gRNA1: GGAGACATATTTGATTTAAAAGG | GATGTGATCTATGCCCGTCTCTGG.

A two-step molecular cloning with Golden Gate assembly method was used, closely following the established Yamamoto protocol.[26] In brief, the assembly vectors (px330S) and destination vector (px330A_1x3/1x4) were separately digested (BpiI) and ligated (Quick ligase) with diluted oligos in single-step reaction mix to generate px330S_C, px330S_T, px330S_S and px330A_1x4_K, px330A_1x3_C,

respectively. Next, the assembly and destination vectors were digested (Eco31I) and ligated (Quick ligase) together according to final multiplex vector in single-step reaction mix. The insertion of gRNA was confirmed in extracted DNA from bacterial colonies (XL1-blue E.coli) via Sanger sequencing using CRISPR step2 Fwd and Rev primers (Fwd: GCCTTTTGCTGGCCTTTTGCTC | Rev: CGGGCCATTTACCGTAAGTTATGTAACG).

Lipofection: Cultured cells (HEK293T, primary ductal cells) were plated for transfection in six experimental arms using 24-wells, each well contained minimum of $5x10^4$ cells cultured in 250µl complete growth medium. Lipofectamine 3000 kit (Fisher scientific) was used to perform transfection experiments following the manufacturer's instructions. After 4h incubation, lipofectamine reagent was replaced with complete growth media.

T7E1 assay: Target cutting was detected using the T7 Endonuclease I Kit (Fisher Scientific) in accordance with the manufacturer's instructions. Briefly, primers were designed to generate amplicons of around 400-500bp. We designed primers such that the predicted cleavage site was not in the center of the amplicon and the detection reaction yields two variable sized band products. Amplified amplicon was digested with 1ul T7 Endonuclease for 15min at 37°C. The reaction was quenched using 1µl of 0.5M EDTA and products detected with electrophoresis on a 2% agarose gel (30min; 150V).

Immunoblotting: The cell pallets from the cell lines were washed with DPBS, resuspended in RIPA buffer and incubated on ice for 30min. The cell lysate was collected after 15min centrifugation at ~15,000rpm. Protein sample concentrations was determined using BCA assay (Fisher Scientific). Gel cassette was loaded with 20ug protein lysate and run with 90V for ~100min until loading dye reached bottom of the gel. Trans-blot turbo cassette (Bio Rad) was used to transfer protein onto membrane. Membrane was washed and blocked with BSA blocking buffer. Appropriate dilutions of primary (1:200 anti-human CDKN2A/p16INK4a, Abcam | clone EPR1473; 1:200 anti-human TP53, Abcam | clone DO-1; 1:200 anti-human SMAD4, Abcam | clone EP618Y) and suitable secondary antibodies in blocking buffer were applied and each incubated for 12h at 4°C.

Immunofluorescence: The cell lines were seeded into Nunc Lab-Tek II Chamber Slide™ System (Fisher Scientific) with 10^4 cells per well and cultured for 3 days at 37°C and 5% CO_2. The confluent cells were washed with PBS, fixed with 4% PFA/PBS and permeabilized with 0.2% Triton/TBST. Following an overnight incubation using the primary antibody solution (1:200 anti-human panCK19, Santa Cruz Biotechnology | clone RCK108; 1:200 anti-human vimentin, Abcam | clone EPR3776), a further 2h incubation with a suitable secondary antibody was conducted. Slides were then washed with 0.5% TBST and then stained with DAPI solution (1:1000).

Immunohistochemistry: Paraffin embedded cell blocks from cell lines were constructed using $1\text{-}2x10^7$ cells fixed in 4% PFA/PBS. Tissue slices were generated and deparaffinized in xylene and hydrated in EtOH. The tissue slices were treated with a hot (100°C) citrate acid retrieval buffer. After cooling, peroxidase solution (1:10) and protein blocking solution were applied for 10min, respectively. Incubation

with antibody solutions (1:200 anti-human CDKN2A/p16INK4a, Abcam | clone EPR1473; 1:200 anti-human TP53, Abcam | clone DO-1; 1:200 anti-human SMAD4, Abcam | clone EP618Y) for 2-3h, was followed by Poly-HRP anti-rabbit/anti-mouse IgG for 30min and Apply DAB (3,3'-Diaminobenzidin) for 10min. Finally, the cell nuclei were stained with 20% hematoxyline for 2min.

Cell Proliferation assay: Cell lines were cultured overnight as replicates in flat-bottom 96-well containing $3x10^3$ cells. The CellTiter96 Aqueous Non-Radioactive Cell Proliferation Assay (MTS) (Promega) kit was used. The MTS and the PMS Solution were thawed an then aliquoted at 20:1 ratio to each well. After incubation (2.5h) the absorbance was measured on microplate reader at wavelengths between 450nm and 540nm. The SkanIt Software Research Edition generated the curve parameters following normalization by tx/t0, while growth curve was plotted using the GraphPad program.

Migration/Invasion assay: Corning® BioCoat® Invasion Chambers with 8.0 µm PET Membrane were used in conjunction with (invasion assay) or in the absence of (migration assay) Matrigel® following the manufacturer's instructions. First, receiver wells were filled with suitable attractant (FBS for carcinoma cell lines, EGF/BPE for HPDE or duct cell lines). For rehydration, 500µl pre-warmed culture medium (DMEM or RPMI w/o FBS; SFM-Keratinocyte Medium w/o EGF/BPE) was added the inserts and incubated for 2h. Medium was replaced with cell suspension ($1x10^5$ cells/insert) in complete growth medium (DMEM or RPMI w/o FBS; SFM-keratinocyte medium w/o EGF/BPE) and transferred into a receiver well with attractant. Matrigel® invasion or migration chambers were incubated for 72h in the cell culture incubator (37°C , 5% carbon dioxide, 95% relative humidity). Non-invading cells were removed by washing with PBS. Cells on bottom-side of the membrane were fixed with 10% Formalin/PBS for 30min and subsequently stained with 0.2% crystal violet in 10% ethanol. The membranes were cover slipped and 3-5 images per cell line at 20-fold magnification were obtained and analyzed. Invasion and migration assays for each cell line were completed in triplicate and repeated three times.

Soft agar assay: A two-layer agar assay was conducted as detailed previously.[18] Briefly, the bottom layer-agar was generated by adding 1.2g to 100ml (1.2%) of diH2O and the top-agar by adding 0.7g to 100ml (0.7%) of diH2O. Subsequently, a gel-medium was generated at 42°C with concentrated (2x) complete growth medium. 1ml from 1.2% base-agar was added to each well of 6-well-plate and cooled at RT until solidified. Now 1ml from the top-gel medium mixture (0.7%) was resuspended 1:1 with cell suspension ($3x10^3$/ml) and plated to each well until solidified. Complete growth medium was added and cell clusters were cultured for 6 weeks. After visible colony formation in positive controls, cells were stained with 0.01% crystal violet for 1h and washed after. Pictures were taken with inverted microscope. The assay was completed in triplicate for each cell line and repeated three times.

Clonogenic assay: To establish an even baseline, 2ml cell suspensions with 200cells/ml from each cell lines were evenly plated as triplicates onto 6-well plates. The cells were cultured for three weeks, during which the culture medium was regularly exchanged (1-2/week). The washed cells were then stained and fixed with 0.5% crystal violet/ethanol for 30min. Lastly, the cell colonies were washed with ddH20 and air dried. Photographs of the wells were obtained using a digital camera.

Cytotoxicity testing: For set-up, transparent flat-bottomed 96-wells were used. We transferred ≈30cells/well in triplicates for each cell line. Based on pre-experiments, distinct gradients of drug concentrations were applied in carcinoma cell lines (0μM, 5μM, 15μM, 45μM, 135μM, 405μM, 1215μM, 3645μM, and 10935μM) and normal cell lines (0μM, 0.2μM, 0.4μM, 0.8μM, 1.6μM, 3.2μM, 6.4μM, 12.8μM, 25.6μM, and 51.2μM). The cells were cultured for 72h with drug and the remaining viable tumor cells (OD value) were used to calculate the inhibition rate (mean OD value of the experimental group/mean OD value of the blank group) at each drug concentration. The data was standardized by tx/t0, and the curves were generated by GraphPad Prism. The EC50 (half maximal effective concentration) value of each cell lines was calculated.

Sanger sequencing: The target regions were amplified by PCR and gel electrophoresis was performed to purify specific bands. The samples were submitted to Eurofins, and Mix2Seq Kit was used for sequencing. Target primer sequences used were: KRAS FWD: CATGGACCCTGACATACTCCC | KRAS REV: ACACGTCTGCAGTCAACTGG; CDKN2A FWD: TCTGTGCTGGAAAATGAATGCTC | CDKN2A REV: GGTAATTAGACACCTGGGGCTTG; TP53 FWD: CACGCACCTCAAAGCTGTTC | TP53 REV: CCTCATCTTGGGCCTGTGTT; SMAD4 FWD: TGAGTTGGTAGGATTGTGAGGATT | SMAD4 REV: TGCTTTCCATCTTATTTCTCAAAAACA

NGS sequencing: Whole exome sequencing was conducted at Eurofins Genomics using the Illumina NovaSeq 6000 platform according to diagnostic criteria (ISO 17025) at an average depth of >30x. The raw sequencing data from Eurofins were in FASTQ format. The VarScan2 pipeline was used for alignment to reference genome GRCh37/hg19 and to generate high-quality filtered BAM files. Candidate mutations were identified using following inclusion criteria: (1) variant allele frequencies of at least 10% of the total reads; (2) ≥30X coverage depth at the variant locus; (3) balance ratio (the ratio of the number of forward reads with the variant to the number of reverse reads with the variant, or vice versa) of the candidate mutation calls was 0.2 or greater; (4) PHRED quality score >25; (5) exclusion of synonymous and non-coding variants. Additionally, each putative somatic mutation was visually inspected using Integrative Genomics Viewer v2.3 (IGV; Broad Institute) for filtering artifactual calls.

Nanopore sequencing: A DNA Fragmentation Kit and gel electrophoresis was used to assess DNA size, while samples with DNA fragment size (>500kbp) were selected. Ligation Sequencing Kit (LSK) was used to perform end repairs for connection of DNA samples of sequencing adapters to form the DNA library. Samples were sequenced using the Rapid Sequencing Kit (SQK-RAD) using the MinION platform from Oxford Nanopore Technologies. LSK109 and LSK110 (ligation-based library preparation without prior DNA fragmentation) were used. Libraries were generated according to the manufacturers protocol (open access on nanoporetech.com/registration required) and loaded on GridION and PromethION flowcells with pore type R 9.4.1. Coverage values and other output information were provided in generated files (.cvg). The AceView profiles generated by a pipeline (ngmlr-samtools-bedtools). The counts were averaged across the window 1 Mbp for GridION and 0.1Mbp and 0.01Mbp for PromethION.

Structural variant analysis: For structural variant (SV) calling, raw data files (.fastq) from Nanopore (shallow sequencing) were aligned to the reference genome (GRCh37/hg19) using the long-read mapper CoNvex Gap-cost alignMents for Long Reads (NGMLR). The output files (.bam) were sorted and indexed with samtools and used for structural variant calling via Sniffles2 (v2.2) with the default parameters (general mode) and reference genome GRCh37/hg19. The output (.vcf) files from Sniffles were filtered using the FILTER tag ('PASS') and INFO tag ('PRECISE') to extract only high-confidence calls with precise breakpoints. The genomic variants were annotated using an ensemble variant effect predictor VEP. The structural variants were classified into simple (insertion, deletion, inversion, duplication) and complex (translocations) variants. For simple and germline variants, SVs < 1kb were excluded from downstream analysis using data manipulation and analysis libraries (python, pandas).[27,28] Circos plots were generated via Circa Genomic Software (http://omgenomics.com/circa).

ecDNA reconstruction: For nanopore sequenced samples, extrachromosomal DNA (ecDNA) detection and reconstruction was performed using Decoil (v1.1.2)[29], with decoil-pipeline sv-reconstruct mode, parameters --min-vaf 0.1 --min-cov-alt 4 --min-cov 6 --max-explog-threshold 0.01 --fragment-min-cov 6 --fragment-min-size 500, starting with BAM file as input and the reference genome GRCh37/hg19. The reconstructed ecDNA elements were visualized using Decoil-viz (v1.0.3, https://github.com/madagiurgiu25/decoil-viz) and annotated using GENCODE V19.

Statistical analysis: The data were expressed as mean ± standard deviation (SD), while the number of experimental repetitions (n) was provided. ImageJ software was used to count cells. GraphPad Prism 8 (GraphPad Software, Boston, MA) was utilized for the generation of charts and the conduction of statistical analyses. The data was first characterized for normal distribution using histogram and conducting the Shapiro–Wilk test and Kolmogorov-Smirnov test. The paired, two-tailed t-test was used with normal distribution, otherwise the Wilcoxon matched pairs signed rank test was used. Differences were considered significant when the p-value was smaller than 0.05. * stands for $p < 0.05$.

Results

Multiplexed gene modification of pancreatic carcinoma driver genes

Early oncogenic activation of the *KRAS* gene is thought to be followed by either sequential or simultaneous inactivation of tumor suppressor genes (*CDKN2A, TP53, SMAD4*) during pancreatic tumorigenesis.[4,30] To investigate the requirement for and timing of driver gene alterations *in vitro*, we constructed CRISPR/Cas9 plasmids using a Golden Gate assembly method that is capable of targeting multiple driver genes at once (**Figure 1A, Suppl. table 1**). Vectors with a variety of gRNA combinations were first tested in easy-to-transfect cells (HEK293T). All gRNAs showed moderate to high on-target cleavage efficiencies (**Figure 1B**). Subsequently, we demonstrated successful derivation of monoclonal gene knock-outs for all vector combinations targeting the main tumor suppressor genes (**Figure 1C**). Unsurprisingly, comparative analyses of knock-out clones revealed that their phenotypes and growth-rates were unaffected, suggesting that HEK293T cells are driven by distinct evolutional patterns (**Figure**

1D). Efforts to insert gene knock-in modeling oncogenic *KRAS*^{G12D} mutation demonstrated low HDR target efficiency (<2%) with a high degree of NHEJ events (16.1%), which challenged its successful clonal derivation (**Figure 1E, Suppl. table 2**). Also recent protocols for base-editing could not yield positively-edited clones due to sensitive ductal cells exposed to electroporation (**Suppl. fig. 1**). These data indicate that pancreatic cancer driver genes can be effectively targeted simultaneous or sequential through multiplexed vectors.

Figure 1. Effective driver gene editing via Golden Gate assembly for generation of multiplexed vectors. A. Schematic flow chart of two-step cloning with Golden Gate assembly method (assembly and destination vector) following the Yamamoto protocol.[26] This resulted in combinatorial vectors (px330A_1x3/1x4) that intracellularly express gRNAs targeting main pancreatic driver genes (*KRAS, CDKN2A, TP53, SMAD4*) and Cas9 for double stranded DNA breaks (DSB). Vectors harbor antibiotic selection markers (A=Ampicillin; S=Spectomycin) for bacterial transformation. **B.** Estimated gene targeting efficiency in HEK293T cells using the T7E1 assay (left). Sanger sequencing confirmed frameshift alterations close to the PAM sequence (right). **C.** Following single-cell cloning protocols, monoclonal cell lines were derived from HEK293T with single-, double or triple knock-out (protein expression) of main tumor suppressors *CDKN2A*, *TP5*3 and *SMAD4* **D.** Top: Phase contrast images of confluent HEK293T clones depicts an unaffected phenotype. Bottom: Growth rate of plated HEK293T cloneswere not influenced by gene knock-out measured by MTS assay (OD value). **E.** NGS results via IGV (Integrative genomics viewer) following transfection of px330A_1x4_K in HEK293T cells. Both, NHEJ (frameshift) and HDR with integration of SNV (KRAS^{G12D}) occurred, while the latter was detected at very low frequency (<2%).

Targeting driver genes in primary duct epithelial cells for natural selection of modified clones

The objective of this study was to investigate the *ex vivo*, molecular requirements for duct cell immortalization by targeting driver genes known to induce pancreatic carcinogenesis. We hypothesized that sub-clonal targeting of tumor suppressor genes in healthy normal ductal cells bears a significant fitness advantage with clonal outgrowth (natural selection). Fresh normal pancreatic ductal tissue was collected, dissected, and digested, and the resulting single ductal cells were split into six experimental arms (**Figure 2A, Suppl. fig. 2**). The KRAS targeting gRNA was excluded from the constructed multiplexed vectors (px330_1x3) due the high rate of NHEJ mediated KRAS knock-outs, which could affect clonal outgrowth. Following a period of 1-2 weeks of tissue culture in collagen-coated 24-well plates, a scattered growth of epithelial islands could be observed under the microscope (**Figure 2B**). To prevent cellular stress and senescence (p16 activation), early and simultaneous transfection was conducted in all experimental arms. Following a period of 3-6 weeks of culture, we found outgrowth in three independent samples (PD47, PD51, PD62) in arms 5 and 6, while epithelial cells in arms 1-4 exhibited signs of cellular senescence and died (**Figure 2C, Table 1**). Of the 71 individual patients with pancreatic duct available for derivation, 11 samples yielded a sufficient number of cells for subsequent transfection. Outgrowth was observed in three individual patient samples, indicating immortalization efficiency of around 27.3% (**Suppl. table 3**). The clinical indication for surgery in the successfully immortalized examples were presence of non-invasive SPN (PD47), NET (PD51) and branch-duct IPMN (PD62),

respectively. The duct tissues were processed from a pathologically confirmed, tumor-free resection margin. NGS analysis (WES, >30x) of the non-involved pancreatic duct samples solely detected the germline variant in *TP53* p.P33R (rs1042522), known to be prevalent SNP in the general population (**Suppl. table 4**). No other genomic alteration in pancreatic driver genes (including the *KRAS* hotspot) or other cancer related genes were detected. All of the outgrown clones were continuously cultured for >30 passages and >280 days, suggesting cellular immortalization via CRISPR-based gene targeting. To the best of our knowledge, this represents the first study to demonstrate successful pancreatic duct cell immortalization using CRISPR-based methodologies.

Figure 2. Natural selection of primary pancreatic ductal cells. A. Primary pancreatic ducts were collected, processed and growing duct cell islands were subsequently transfected with constructed multiplexed vectors in six experimental arms (px330A_1x3, px330A_1x3_C, px330A_1x3_T, px330A_1x3_S, px330A_1x3_CT, px330A_1x3_CTS). **B.** Characteristic pancreatic ductal island with cobblestone-like arrangement following 4-10 days culture. Scale bar=100mm. **C.** Following continuous culture, outgrowth of pancreatic ductal cells was observed in experimental arms 5 ($px330^{CDKN2A/TP53}$) and 6 ($px330^{CDKN2A/TP53/SMAD4}$), not in others.

Characterization of immortalized duct precursor cell lines

All immortalized duct cell lines were subjected to continuous observation and in-depth characterization. Bright-field microscopy revealed that the cells exhibited characteristic cobblestone-like growth patterns similar to those observed in other immortalized duct cell lines (**Figure 3A**). Throughout, the cell lines consistently exhibited the same STR fingerprints of their originating tissue (**Suppl. table 5**). They expressed an identifying cellular marker of duct epithelial cells (CK19), while mesenchymal markers were not expressed (**Figure 3B**). Normalized growth curves following colorimetric measurements (MTS assay) showed intermediary cellular growth compared to controls, indicating precursor cell biology ($p>0.05$, **Figure 3C**). Still, there were statistically significant differences in Ki67 indices in PD51CT ($p<0.001$), PD51_CTS ($p<0.001$) and PD62_CT ($p=0.0018$) compared to HPDE (**Figure 3D**). We demonstrated monoclonal tumor suppressor knock-out of targeted driver genes *CDKN2A* and *TP53*, while there was only “knock-down” (reduced protein expression) of *SMAD4*, suggesting that duct cell immortalization was primarily driven by knock-out of regulators of cell cycle progression (**Figure 3E**). We further investigated cell line growth under three-dimensional culture conditions using standardized protocols for organoid culture and innovative decellularized tissue slices.[24,31] In both, we observed duct cell clusters, whereby cluster growth appeared slowed or absent compared to PDAC-derived tumoroids (**Figure 3F**). Interestingly, organoid growth could be manipulated with Nutlin treatment and Noggin removal, highlighting the niche dependence of the genetically modified clones (**Figure 3G**). Overall, we demonstrated maintained duct cell characteristics in the long-term culture of novel immortalized duct cell lines.

Figure 3. Characterization of immortalized primary duct cell lines. A. Phase contrast images of novel gene modified pancreatic duct (PD) cell lines depicted their duct epithelial phenotype. **B.** Markers of

differentiation further characterized their ductal origin ($CK19^{+}Vim^{-}$). **C.** Growth rates following absorbance measurements via MTS assay resembled that of $HPDE^{E6E7}$ cell line, but was decelerated compared carcinoma cell lines (e.g. AsPC1). **D.** The proliferation index following IHC analyses showed a significant increase in gene modified cells (PD51_CT, PD51_CTS, PD62_CT). **E.** Complete knock-out was observed for p53 and cdkn2a protein in cell line pools, while only reduced protein expression was observed in smad4. As control (C) normal pancreatic duct tissue was used with retained expression. **F.** Top: In three-dimensional cell culture we observed less infiltrative and smaller tumoroids in precursor- compared to carcinoma cell lines. Bottom: H&E images from sliced, decellularized tissue matrices showed cluster growth solely in carcinoma cell lines (arrows), not in modified ductal cell lines. **G.** Noggin removal or Nutlin treatment during 3-week culture resulted in positive selection of *TP53* and *SMAD4* modified cell lines, while negative selection occurred in $HPDE^{E6E7}$.

Invasive properties of novel duct epithelial precursor cell lines

To determine the degree of invasiveness and malignancy of our novel immortalized pancreatic duct cell lines, we performed *in vitro* tumorgenicity assays. First, we assessed their colony-forming capacity. In a modified clonogenic assay, we showed that cells form significantly fewer colonies than pancreatic cancer cell line controls, with colony-forming capacity similar to that of the pancreatic duct cell line control ($p<0.001$, **Figure 4A**). Furthermore, when seeding cells in soft agar (soft agar assay), we could show that carcinoma cells form cell clusters following six weeks of culture, while our novel immortalized pancreatic duct cell lines and the pancreatic duct cell line control were not able to form cell clusters ($p<0.001$, **Figure 4B**). To further elucidate their invasive potential, we also conducted migration and invasion assays. Both PDAC cell lines (Panc1, AsPC-3) showed an overall higher degree of migration and invasion, compared to the novel immortalized ductal cell lines (**Figure 4C**). Altogether, the invasion index was significantly lower in the novel immortalized duct cell lines compared to the pancreatic ductal adenocarcinoma cell lines ($p<0.001$). Despite immortalization, *in vitro* assessment of classic tumorigenic features highlighted rather non-invasive characteristics in novel gene-modified duct cell lines. This may make them a particularly interesting resource to investigate precursor cell biology. Lastly, we sought to analyze the impact of driver gene alterations on cellular resistance toward current chemotherapy agents used for pancreatic cancer treatment. We performed cytotoxicity assays for oxaliplatin and irinotecan treatment (**Figure 4D**) and found that IC50 values across the novel immortalized duct cell lines ($p<0.001$), as well as the pancreatic duct cell line control ($p<0.001$) were significantly lower than that of the PDAC cell lines assayed. These data indicate that molecular resistance may be transmitted through signatures beyond alterations in specific driver genes.

Figure 4. Tumorigenicity assessment of precursor cell lines. A. Modified clonogenic assay showed accelerated colony formation in carcinoma compared to precursor cell lines. **B.** Colony formation in soft agar environment was present in carcinoma but not in precursor cell lines. **C.** Invasion index was measured following migration (PET membrane) and invasion (Matrigel coated) assay in their respective chemoattractant. **D.** Cytotoxicity assay demonstrated increased IC50 values in carcinoma- compared to precursor cell lines following oxaliplatin and irinotecan treatment.

Molecular evolution in genomic signatures of novel precursor cell lines in vitro

To gain better understanding of the molecular signatures of our novel immortalized ductal cell lines, we conducted long-read Nanopore sequencing and short-read WES. To identify germline variants, we also sequenced DNA from the uninvolved normal pancreatic tissue. The Nanopore analyses revealed that all the precursor cell lines harbor a diploid karyotype across the genome, while AsPC1, PANC-1 and also HPDE cells showed increased copy numbers at several loci (**Figure 5A**). Expected somatic mutations in *CDKN2A*, *TP53*, *SMAD4*, but also other somatic alterations were present in the novel immortalized cell lines by WES (**Table 2**). Most of the detected SNVs were localized in coding regions of non-cancer related genes (e.g. *RHOJ, TCF20, FOXN4*) and were sub-clonal indicated by lower variant allele frequencies (VAF). Importantly, we identified the CRISPR-based modifications in the driver genes *CDKN2A*, *TP53, and SMAD4* with moderate to high VAF (**Figure 5B**). No somatic mutations were identified in *KRAS* in any of the novel immortalized cell lines. The uniformly high VAF (>0.8) in *CDKN2A* and *TP53* suggests that these gene modifications were responsible for clonal expansion and that either bi-allelic loss (e.g. PD51_CT) or loss-of-heterozygosity (LOH) was mandatory (e.g.PD47_CTS, PD51_CT, PD51_CTS, PD62_CT, PD62_CTS). By contrast, concomitant somatic mutations showed lower VAFs (VAF<0.7) and were thus acquired later during the immortalization process. Except alterations in *CDKN2A*, *TP53*, and *SMAD4*, the majority of concomitant alterations were not shared between samples of the same origin (**Figure 5C**). Still, samples originating from the same tissue specimen maintained a high Jaccard coefficient, indicating their mutual ancestors when including their somatic and germline variants (**Figure 5D**). Next, we sought to explore the impact of driver gene alterations on deterministic patterns and genome instability during temporal pancreatic carcinogenesis. We conducted WES and Nanopore sequencing at two distinct evolutionary time points (passages 10 and 25) following the multiplexed driver gene targeting. We found cell lines acquired genomic aberrations over time, including SNVs and focal copy number changes (**Figure 5E, Suppl. table 6)**. Consequently, we analyzed the nanopore long-read data to further characterize simple and complex structural variants (SVs) (**Suppl. table 7**). Following normalization by chromosomal size, we found that chromosomes 17 and 19 were prominently affected across cell lines at later passages that well corresponds with data from control carcinoma cell lines (**Figure 5F, Suppl. fig. 3, Suppl. fig. 4)**. Complex rearrangements (indicated by BNDs) however occurred primarily at chromosomes 9, 15, 17, 18, with breakpoints in genes known to trigger pancreatic carcinogenesis (*TP53, ALK, RPTOR, MAP2K4, RBM47, NTRK3)* (**Figure 5G)**. Using Decoil[29], we reconstructed extrachromosomal circles (ecDNA) using the long-read sequencing data and found a larger ecDNA that included a candidate oncogene (*MAP2K5*) as a consequence of complex re-arrangements (**Figure 5H**). Although not powered (low sample size) for ultimate assessment, these results support observations on deterministic patterns after bi-allelic *TP53* loss-of-function with downstream complex re-arrangements at specific loci in a human *in vitro* model. We identified few alterations at previously characterized off-target sites in three out of six targeted cell lines, indicating that off-target modifications resulting from the multiplexed design were limited (**Suppl. fig. 5**; **Suppl. Table 8**). Among them, the *CDKN2B* gene is closely related to *CDKN2A* and is known to be similarly involved in the regulation of the cell cycle, while *NID1* is related to cell-matrix interaction. No potential

off-target sites were found in other immortalized cell lines, highlighting their redundancy for the natural selection and immortalization process.

Figure 5. Genomic evolution following driver gene targeting. A. Copy number analyses of generated PD cell lines at earlier passages from long-read data (Nanopore) depicts a diploid karyotype, while carcinoma and HPDE^{E6E7} cell lines reveal relevant number of focal amplifications and deletions. **B.** NGS results (Integrative genomics viewer) from generated PD cell lines confirmed frameshift alterations at the targeted loci from pancreatic driver genes (*CDKN2A, TP53, SMAD4*) close to the PAM sites. **C.** The Venn diagram depicts shared alterations along PD47^{CT}, PD47^{CTS}, PD51^{CT} and PD51^{CTS} cells mirroring the specified Cas9 targeted gene sites. **D.** Calculation of Jaccard coefficient from somatic and germline alterations reveals similarity due to mutual ancestors in CT and CTS clones. **E.** Nanopore long-read sequencing data at later passages (P25) revealed accumulation of focal CNVs. **F.** The histograms characterize fractional structural variants (SVs) across the genome from early (P10) to later passage (P25) with focal hotspots at Chromosome 17 and 19. SVs were normalized to chromosomal size. **G.** Circos plots delineate complex structural rearrangements (translocations, BFB, fold-back inversions) at focal hotspots (Chr9, Chr15, Chr17, Chr18) that affected oncogenes and tumor suppressors. **H.** Using Decoil, a larger circular re-arrangement (ecDNA) could be detected in PD51_CTS.

Discussion

The ongoing debate on cell of origin giving rise to pancreatic duct cell adenocarcinoma appears clinically irrelevant in light of standardized treatment of care for the majority of PDAC patients.[32] However, molecular subtyping of patient tissue may soon establish individualized treatment concepts. Human data suggest that both, acinar as well as pancreatic ductal cells can participate in the carcinogenic process.[33] We have developed a versatile model that may help us to understand the requirements of loss-of-function gene targeting for duct cell immortalization, as a strong surrogate of uncontrolled tumor growth *in vivo*. Although oncogenic activation via *KRAS*^{mut} alterations likely poses an indispensable growth signal for pre-malignant cells *in vivo*, we primarily focused on characterizing the phenotypic consequences of main tumor suppressors from transiently transfected normal duct cells considering the poor efficiency of HDR when using the CRISPR/Cas9 technology. We successfully employed multiplexed genome engineering of main tumor suppressors in various combinations, to assess early carcinogenic features on targeted cells and evaluate downstream deterministic patterns.

To demonstrate the feasibility of our approach, we have generated multiplexed vectors following a Golden Gate assembly method (Yamamoto´s Lab protocol) which allows for the simultaneous transport of up to four gRNAs into both cell lines and primary cells. The vectors performed well in easy-to-transfect cells (HEK293T) and appeared suitable for testing our hypothesis on genomic requirements for duct cell immortalization in primary cells. Repeated experimental set-ups allocating the harvested and viable primary ductal cells into six experimental arms, convincingly demonstrated that the combination of *CDKN2A*^{mut} and *TP53*^{mut} is an absolute requirement for sustained growth for this epithelial cell type in

two-dimensional tissue cultures. At genomic level, highest VAFs as well as complete protein knock-out were detected for these tumor suppressors in the generated PD cell lines, highlighting the role of bi-allelic loss or LOH for perversive clonal expansion of pre-neoplastic cells.[34] In stark contrast, the concomitant *SMAD4*^{mut} did not fully penetrate and only resulted in “knock-down” (reduced bulk protein expression) and low VAF in the targeted cells. Still, *SMAD4*^{mut} conveyed a survival advantage over time, reflected by increasing VAF from early (P10) to later passages (P25). This is not surprising, as loss of function of both, p16 and p53 harbor the inherent potential to overcome cellular senescence, while abrogated TGF-ß signaling has no direct gatekeeper effect on the cell cycle, but transmits unresponsiveness towards inhibiting autocrine TGF-ß.[35,36] Other studies showed that epithelial cells from airway or prostate tissue could be immortalized via *CDKN2A* targeting but only in co-expression with telomerase subunit hTERT, which can overcome crisis at higher passages.[22,37] The attenuation of p53 (and Rb) prevents cellular arrest and has been a successful concept for viral E6E7 immortalization strategies in pancreatic ductal cells.[14] A combination silencing strategy (shRNA TP53, CDKN1A) successfully established immortalized and functional megakaryocyte progenitor cells.[38] To our knowledge, no other successful immortalization attempt via CRISPR-based driver gene targeting has been reported in pancreatic ductal cells.

The novel PD cell lines were observed to maintain a characteristic duct cell phenotype with sustained proliferation capacities, similar to that of HPDE^{E6E7} cells. In three-dimensional Matrigel domes submerged in pancreatic expansion media, the dispersed single ductal cells effectively generated organoids that may suggest the presence of some maintained stem cell-like features.[24,39] This could be manipulated via genotype-dependent agents (Nutlin3a, Noggin-removal) likely further selecting the more proliferative, gene-modified clones mirrored by enhanced sizes of cell clusters.[20,40] In any case, *in vitro* assays demonstrated low colony-forming and migratory/invasive capacity as well as maintained anchorage dependence. The data positions the established PD cells in a precursor-like category. In contrast to our expectations and despite exhibiting only moderate proliferation indices, PD cells display marked chemo-sensitivity, while IC50 values in pancreatic carcinoma cell lines were significantly higher. Low IC50 values in HPDE cells have been reported previously.[41] This may be linked to p53-mediated mismatch repair mechanisms, manipulated at protein level in HPDE^{E6E7} and genetically in PD cell lines.[42] Chemotherapy-induced synthetic lethality was likely responsible for this effect, while more complex genomic aberrations in PDAC cells confer resistance towards these reagents.[43] Genetically defined precursor cell models are helpful when investigating precursor cell biology *in vitro*, characterizing factors that may tilt the balance towards carcinoma development or illuminate molecular determinants for therapy resistance.

The role of loss of heterozygosity (LOH) in *TP53* mutated cancer cells has recently been revisited in lineage tracing murine experiments and human organoid culture.[11,34] Deterministic focal chromosomal rearrangements are likely responsible for subsequent complex structural aberrations or even chaotic polyploidization typically found in invasive and metastatic carcinoma cells.[44] We could confirm similar

observations in our human culture model from a patient-derived, diploid ductal cell resource: Following the transient targeting of a specified driver gene loci of *TP53* and *CDKN2A*, complex chromosomal events occurred over time concomitant with accumulation of SNVs. This was replicated in individual patient samples (CT vs CTS) while retaining a high similarity index (Jaccard coefficient) underscoring CRISPR-mediated modelling of such deterministic structural or numerical events. At later passages, we observed recurrent amplifications (CNV), simple as well as complex structural variants in chromosomes 9, 15, 17 and 19. Recurrent structural losses were apparent in chromosomes 10 and 13. Also, unique structural changes occurred, which potentially implicate distinct biological consequences and inter-tumoral heterogeneity. On the other hand, downstream complex BNDs likely provoked ecDNA generation (PD51_CTS) in our model that warrants further mechanistic investigation in the role of ecDNA in PDAC.

In the presented study, we propose a relevant model to investigate deterministic patterns of cancer evolution derived from distinct duct epithelial cell resources. We believe that this model may help to better define mutual requirements for cellular invasion.

Nevertheless, several limitations in our study remain. First, it should be noted that all experiments were conducted exclusively *in vitro,* and therefore the specific features of *in vivo* carcinoma growth were not recapitulated. In order to gain insights into the phenotypic hallmarks of carcinoma cells, such as invasion and proliferation, we performed culture assays as replacement methodology. It is not possible to definitively rule out the possibility that these cells grow in transplanted animal models or even possess capabilities to metastasize. Besides, the molecular determinants of duct cell immortalization outlined in this study may putatively be counteracted *in vivo* via interaction with the tumor microenvironment (stroma, immune cells). In addition, the relevance of oncogenic *KRAS* activation for early pancreatic carcinogenesis remains indisputable but could not be modeled thus far. The advancements of modern knock-in concepts will likely facilitate the precise introduction of hotspot alterations or other SNVs *in vitro* enabling a more accurate representation of pancreatic carcinogenesis.[45] Nevertheless, low viability with limited numbers of primary ductal cells from fresh resection specimen as well as their strong sensitivity in transfection experiments (e.g. electroporation), renders such endeavors particularly challenging. For now, we believe this may primarily be a technical issue as we could not initiate any meaningful genotype screening in our primary ductal cells. Still, we cannot rule out downstream biological factors that may have additionally prevented genotype enrichment such as oncogenic *KRAS* induced senescence or lack of immunological feedback activation.[46,47]

This study provides a first conceptual framework for CRISPR-based duct cell immortalization allowing downstream modeling of deterministic patterns during pancreatic carcinogenesis. Better understanding of early molecular trajectories of duct cell dysplasia may uncover predictable patterns of pre-invasive cells towards progression of invasive and metastatic subclones. The current knowledge on genomic and transcriptional changes during early tumorigenesis (precursor stage) in humans are predominantly derived from snap-shot analyses of dysplastic areas (PanIN, IPMN) from either resected or autopsy pancreatic tissue samples. Longitudinal, multi-sampling studies for temporal investigation of pre-

malignant lesions in humans proved impractical or even impossible. Hence, such *in vitro* model could enable real-time observation of earlier evolutionary processes responsible for intra- and inter-lesional heterogeneity. Wider application of this conceptional approach lies in high-throughput derivation and maintenance of healthy mammalian cells in other difficult to transfect tissue types (stem cells, other epithelial tissue types). We believe that this model can be readily reproduced across laboratories, fostering innovation for earlier detection.

Abbreviations

ADM	Acinar-to-duct metaplasia
ATCC	American Type Culture Collection
BAM	Binary Alignment Map
BND	Breakends
BPE	Bovine pituitary extract
CNV	Copy number variation
CRISPR	Clustered regularly interspaced short palindromic repeats
CT	Computed tomography
DAB	3,3'-Diaminobenzidin
ecDNA	Extrachromosomal circular DNA
EGF	Epithelial growth factor
GEMM	Genetically engineered mouse model
HDR	Homology directed repair
IC50	Half-maximal inhibitory concentration
IGV	Integrative Genomics Viewer
IPMN	Intraductal papillary mucinous neoplasms
LOH	Loss of heterozygosity
LSK	Ligation Sequencing Kit
MCN	Mucinous cyst neoplasm
MRI	Magnetic resonance imaging
MTS	Non-Radioactive Cell Proliferation Assay
NGMLR	CoNvex Gap-cost alignMents for Long Reads
NGS	Next generation sequencing
NHEJ	Non-homologous end joining
PAM	Protospacer adjacent motif
PD	Primary duct cell line
PDAC	Pancreatic ductal adenocarcinoma
SD	Standard deviation
SFM	Serum-free media

SNV	Single nucleotide variant
SQK-RAD	Rapid Sequencing Kit
STR	Short tandem repeats
SV	Structural variants
UCSC	University of California genome browser
VAF	Variant allele frequency
VEP	variant effect predictor
WES	Whole exome sequencing

Declarations

Ethics approval

The study was approved by the institutional ethics committee (Charité – Universitätsmedizin Berlin, EA4/108/19). The study was conducted in accordance Declaration of Helsinki International Ethical Guidelines for Biomedical Research Involving Human Subjects (CIOMS), Belmont Report, or U.S. Common Rule.

Consent for publication

Informed consent was obtained from all subjects involved in the study.

Competing interests

All listed authors confirmed that there are no competing interests to declare.

Availability of data and material

All data relevant to the study are included in the article or uploaded as online supplemental information. All cell lines used in this study were authenticated via STR fingerprinting and regularly mycoplasma tested. All NGS data analyzed in the manuscript has been deposited at the European Genome-phenome Archive (EGA), which is hosted by the EBI and the CRG, under accession number EGAD50000001842. Further information about EGA can be found at https://ega-archive.org and "The European Genome-phenome Archive of human data consented for biomedical research."Other data that support the findings of this study are available from the corresponding author upon request.

Funding

M.F. received funding from Else Kröner Fresenius Stiftung (EKFS). M.F., L.T., K.H.H., G.H. are C.N. were fellows of the BIH Charité Clinician Scientist programme, funded by the BIH – Berlin Institute of Health

and the Charité – Universitätsmedizin Berlin. M.F.

Authors contributions

Conceptualization by M.F., L.D.W and N.R.; Methodology conducted via M.H., D.M., A.D., J.T, R.W., C.Z.J., F.D., J.F.S. and M.F.; Software used by M.H., D.M., A.D., J.T. and M.F., Formal analysis by M.H., D.M., A.D., J.T, R.W., C.Z.J., F.D., J.F.S. and M.F., Resources provided by A.H., F.H., A.D., T.M., J.P., I.M.S (Experimentelle Chirurgie), N.R. and L.D.W.; Data curation by M.H. and M.F.; writing original draft preparation by M.H., L.D.W., N.R. and M.F.; Revision and editing by; Supervision by A.H., T.M., J.P., I.M.S. N.R, L.D.W. and M.F.; All authors have read and agreed to the published version of the manuscript.

Acknowledgments

We would like to express our sincerest gratitude to Anja Schirmeier, Kirsten Führer, Steffen Lippert, and Dr. Anja Reutzel-Selke for all the support while organizing, overseeing and managing the laboratories.

References

1. Felsenstein M, Hruban RH, Wood LD. New Developments in the Molecular Mechanisms of Pancreatic Tumorigenesis. *Adv Anat Pathol*. Mar 2018;25(2):131-142. doi:10.1097/PAP.0000000000000172
2. Basturk O, Hong SM, Wood LD, et al. A Revised Classification System and Recommendations From the Baltimore Consensus Meeting for Neoplastic Precursor Lesions in the Pancreas. *Am J Surg Pathol*. Dec 2015;39(12):1730-41. doi:10.1097/PAS.0000000000000533
3. Hruban RH, Adsay NV, Albores-Saavedra J, et al. Pancreatic intraepithelial neoplasia: a new nomenclature and classification system for pancreatic duct lesions. *Am J Surg Pathol*. May 2001;25(5):579-86. doi:10.1097/00000478-200105000-00003
4. Wood LD, Canto MI, Jaffee EM, Simeone DM. Pancreatic Cancer: Pathogenesis, Screening, Diagnosis, and Treatment. *Gastroenterology*. Aug 2022;163(2):386-402 e1. doi:10.1053/j.gastro.2022.03.056
5. Hutchings D, Waters KM, Weiss MJ, et al. Cancerization of the Pancreatic Ducts: Demonstration of a Common and Under-recognized Process Using Immunolabeling of Paired Duct Lesions and Invasive Pancreatic Ductal Adenocarcinoma for p53 and Smad4 Expression. *Am J Surg Pathol*. Nov 2018;42(11):1556-1561. doi:10.1097/PAS.0000000000001148
6. Braxton AM, Kiemen AL, Grahn MP, et al. 3D genomic mapping reveals multifocality of human pancreatic precancers. *Nature*. May 2024;629(8012):679-687. doi:10.1038/s41586-024-07359-3
7. Kopp JL, von Figura G, Mayes E, et al. Identification of Sox9-dependent acinar-to-ductal reprogramming as the principal mechanism for initiation of pancreatic ductal adenocarcinoma. *Cancer Cell*. Dec 11 2012;22(6):737-50. doi:10.1016/j.ccr.2012.10.025

8. Morris JPt, Cano DA, Sekine S, Wang SC, Hebrok M. Beta-catenin blocks Kras-dependent reprogramming of acini into pancreatic cancer precursor lesions in mice. *J Clin Invest*. Feb 2010;120(2):508-20. doi:10.1172/JCI40045
9. Hingorani SR, Wang L, Multani AS, et al. Trp53R172H and KrasG12D cooperate to promote chromosomal instability and widely metastatic pancreatic ductal adenocarcinoma in mice. *Cancer Cell*. May 2005;7(5):469-83. doi:10.1016/j.ccr.2005.04.023
10. Hingorani SR, Petricoin EF, Maitra A, et al. Preinvasive and invasive ductal pancreatic cancer and its early detection in the mouse. *Cancer Cell*. Dec 2003;4(6):437-50. doi:10.1016/s1535-6108(03)00309-x
11. Baslan T, Morris JPt, Zhao Z, et al. Ordered and deterministic cancer genome evolution after p53 loss. *Nature*. Aug 2022;608(7924):795-802. doi:10.1038/s41586-022-05082-5
12. Mueller S, Engleitner T, Maresch R, et al. Evolutionary routes and KRAS dosage define pancreatic cancer phenotypes. *Nature*. Feb 1 2018;554(7690):62-68. doi:10.1038/nature25459
13. Maddipati R, Norgard RJ, Baslan T, et al. MYC Levels Regulate Metastatic Heterogeneity in Pancreatic Adenocarcinoma. *Cancer Discov*. Feb 2022;12(2):542-561. doi:10.1158/2159-8290.CD-20-1826
14. Ouyang H, Mou L, Luk C, et al. Immortal human pancreatic duct epithelial cell lines with near normal genotype and phenotype. *Am J Pathol*. Nov 2000;157(5):1623-31. doi:10.1016/S0002-9440(10)64800-6
15. Qian J, Niu J, Li M, Chiao PJ, Tsao MS. In vitro modeling of human pancreatic duct epithelial cell transformation defines gene expression changes induced by K-ras oncogenic activation in pancreatic carcinogenesis. *Cancer Res*. Jun 15 2005;65(12):5045-53. doi:10.1158/0008-5472.CAN-04-3208
16. Huang L, Holtzinger A, Jagan I, et al. Ductal pancreatic cancer modeling and drug screening using human pluripotent stem cell- and patient-derived tumor organoids. *Nat Med*. Nov 2015;21(11):1364-71. doi:10.1038/nm.3973
17. Hohwieler M, Illing A, Hermann PC, et al. Human pluripotent stem cell-derived acinar/ductal organoids generate human pancreas upon orthotopic transplantation and allow disease modelling. *Gut*. Mar 2017;66(3):473-486. doi:10.1136/gutjnl-2016-312423
18. Felsenstein M, Trujillo MA, Huang B, et al. Generation and characterization of a cell line from an intraductal tubulopapillary neoplasm of the pancreas. *Lab Invest*. Jul 2020;100(7):1003-1013. doi:10.1038/s41374-020-0372-0
19. Huang B, Trujillo MA, Fujikura K, et al. Molecular characterization of organoids derived from pancreatic intraductal papillary mucinous neoplasms. *J Pathol*. Nov 2020;252(3):252-262. doi:10.1002/path.5515
20. Seino T, Kawasaki S, Shimokawa M, et al. Human Pancreatic Tumor Organoids Reveal Loss of Stem Cell Niche Factor Dependence during Disease Progression. *Cell Stem Cell*. Mar 1 2018;22(3):454-467 e6. doi:10.1016/j.stem.2017.12.009

21. Wasserman JS, Fowle H, Hashmi R, et al. Derivation of human primary prostate epithelial cell lines by differentially targeting the CDKN2A locus along with expression of hTERT. *Sci Rep*. Sep 2 2024;14(1):20409. doi:10.1038/s41598-024-71306-5
22. Zhao Z, Fowle H, Valentine H, et al. Immortalization of human primary prostate epithelial cells via CRISPR inactivation of the CDKN2A locus and expression of telomerase. *Prostate Cancer Prostatic Dis*. Mar 2021;24(1):233-243. doi:10.1038/s41391-020-00274-4
23. Maresch R, Mueller S, Veltkamp C, et al. Multiplexed pancreatic genome engineering and cancer induction by transfection-based CRISPR/Cas9 delivery in mice. *Nat Commun*. Feb 26 2016;7:10770. doi:10.1038/ncomms10770
24. Broutier L, Andersson-Rolf A, Hindley CJ, et al. Culture and establishment of self-renewing human and mouse adult liver and pancreas 3D organoids and their genetic manipulation. *Nat Protoc*. Sep 2016;11(9):1724-43. doi:10.1038/nprot.2016.097
25. Hanna RE, Doench JG. Design and analysis of CRISPR-Cas experiments. *Nat Biotechnol*. Jul 2020;38(7):813-823. doi:10.1038/s41587-020-0490-7
26. Sakuma T, Nishikawa A, Kume S, Chayama K, Yamamoto T. Multiplex genome engineering in human cells using all-in-one CRISPR/Cas9 vector system. *Sci Rep*. Jun 23 2014;4:5400. doi:10.1038/srep05400
27. Sedlazeck FJ, Rescheneder P, Smolka M, et al. Accurate detection of complex structural variations using single-molecule sequencing. *Nat Methods*. Jun 2018;15(6):461-468. doi:10.1038/s41592-018-0001-7
28. Chukwu W, Lee S, Crane A, et al. Comparison of germline and somatic structural variants in cancers reveal systematic differences in variant generating and selection processes. *bioRxiv*. Jun 18 2024;doi:10.1101/2023.10.09.561462
29. Giurgiu M, Wittstruck N, Rodriguez-Fos E, et al. Reconstructing extrachromosomal DNA structural heterogeneity from long-read sequencing data using Decoil. *Genome Res*. Aug 21 2024;doi:10.1101/gr.279123.124
30. Notta F, Chan-Seng-Yue M, Lemire M, et al. A renewed model of pancreatic cancer evolution based on genomic rearrangement patterns. *Nature*. Oct 20 2016;538(7625):378-382. doi:10.1038/nature19823
31. Daneshgar A, Klein O, Nebrich G, et al. The human liver matrisome - Proteomic analysis of native and fibrotic human liver extracellular matrices for organ engineering approaches. *Biomaterials*. Oct 2020;257:120247. doi:10.1016/j.biomaterials.2020.120247
32. Khorana AA, McKernin SE, Berlin J, et al. Potentially Curable Pancreatic Adenocarcinoma: ASCO Clinical Practice Guideline Update. *J Clin Oncol*. Aug 10 2019;37(23):2082-2088. doi:10.1200/JCO.19.00946
33. Cui Zhou D, Jayasinghe RG, Chen S, et al. Spatially restricted drivers and transitional cell populations cooperate with the microenvironment in untreated and chemo-resistant pancreatic cancer. *Nat Genet*. Sep 2022;54(9):1390-1405. doi:10.1038/s41588-022-01157-1

34. Karlsson K, Przybilla MJ, Kotler E, et al. Deterministic evolution and stringent selection during preneoplasia. *Nature*. Jun 2023;618(7964):383-393. doi:10.1038/s41586-023-06102-8
35. Morton JP, Timpson P, Karim SA, et al. Mutant p53 drives metastasis and overcomes growth arrest/senescence in pancreatic cancer. *Proc Natl Acad Sci U S A*. Jan 5 2010;107(1):246-51. doi:10.1073/pnas.0908428107
36. Sharpless NE, Sherr CJ. Forging a signature of in vivo senescence. *Nat Rev Cancer*. Jul 2015;15(7):397-408. doi:10.1038/nrc3960
37. Smith JL, Lee LC, Read A, et al. One-step immortalization of primary human airway epithelial cells capable of oncogenic transformation. *Cell Biosci*. 2016;6:57. doi:10.1186/s13578-016-0122-6
38. Sone M, Nakamura S, Umeda S, et al. Silencing of p53 and CDKN1A establishes sustainable immortalized megakaryocyte progenitor cells from human iPSCs. *Stem Cell Reports*. Dec 14 2021;16(12):2861-2870. doi:10.1016/j.stemcr.2021.11.001
39. Boj SF, Hwang CI, Baker LA, et al. Organoid models of human and mouse ductal pancreatic cancer. *Cell*. Jan 15 2015;160(1-2):324-38. doi:10.1016/j.cell.2014.12.021
40. Kucab JE, Hollstein M, Arlt VM, Phillips DH. Nutlin-3a selects for cells harbouring TP53 mutations. *Int J Cancer*. Feb 15 2017;140(4):877-887. doi:10.1002/ijc.30504
41. Cui Y, Brosnan JA, Blackford AL, et al. Genetically defined subsets of human pancreatic cancer show unique in vitro chemosensitivity. *Clin Cancer Res*. Dec 1 2012;18(23):6519-30. doi:10.1158/1078-0432.CCR-12-0827
42. Lin X, Howell SB. DNA mismatch repair and p53 function are major determinants of the rate of development of cisplatin resistance. *Mol Cancer Ther*. May 2006;5(5):1239-47. doi:10.1158/1535-7163.MCT-05-0491
43. McLornan DP, List A, Mufti GJ. Applying synthetic lethality for the selective targeting of cancer. *N Engl J Med*. Oct 30 2014;371(18):1725-35. doi:10.1056/NEJMra1407390
44. Bielski CM, Zehir A, Penson AV, et al. Genome doubling shapes the evolution and prognosis of advanced cancers. *Nat Genet*. Aug 2018;50(8):1189-1195. doi:10.1038/s41588-018-0165-1
45. Anzalone AV, Koblan LW, Liu DR. Genome editing with CRISPR-Cas nucleases, base editors, transposases and prime editors. *Nat Biotechnol*. Jul 2020;38(7):824-844. doi:10.1038/s41587-020-0561-9
46. Serrano M, Lin AW, McCurrach ME, Beach D, Lowe SW. Oncogenic ras provokes premature cell senescence associated with accumulation of p53 and p16INK4a. *Cell*. Mar 7 1997;88(5):593-602. doi:10.1016/s0092-8674(00)81902-9
47. Lee KE, Bar-Sagi D. Oncogenic KRas suppresses inflammation-associated senescence of pancreatic ductal cells. *Cancer Cell*. Nov 16 2010;18(5):448-58. doi:10.1016/j.ccr.2010.10.020

Tables

Tables are available in the Supplementary Files section.

Figures

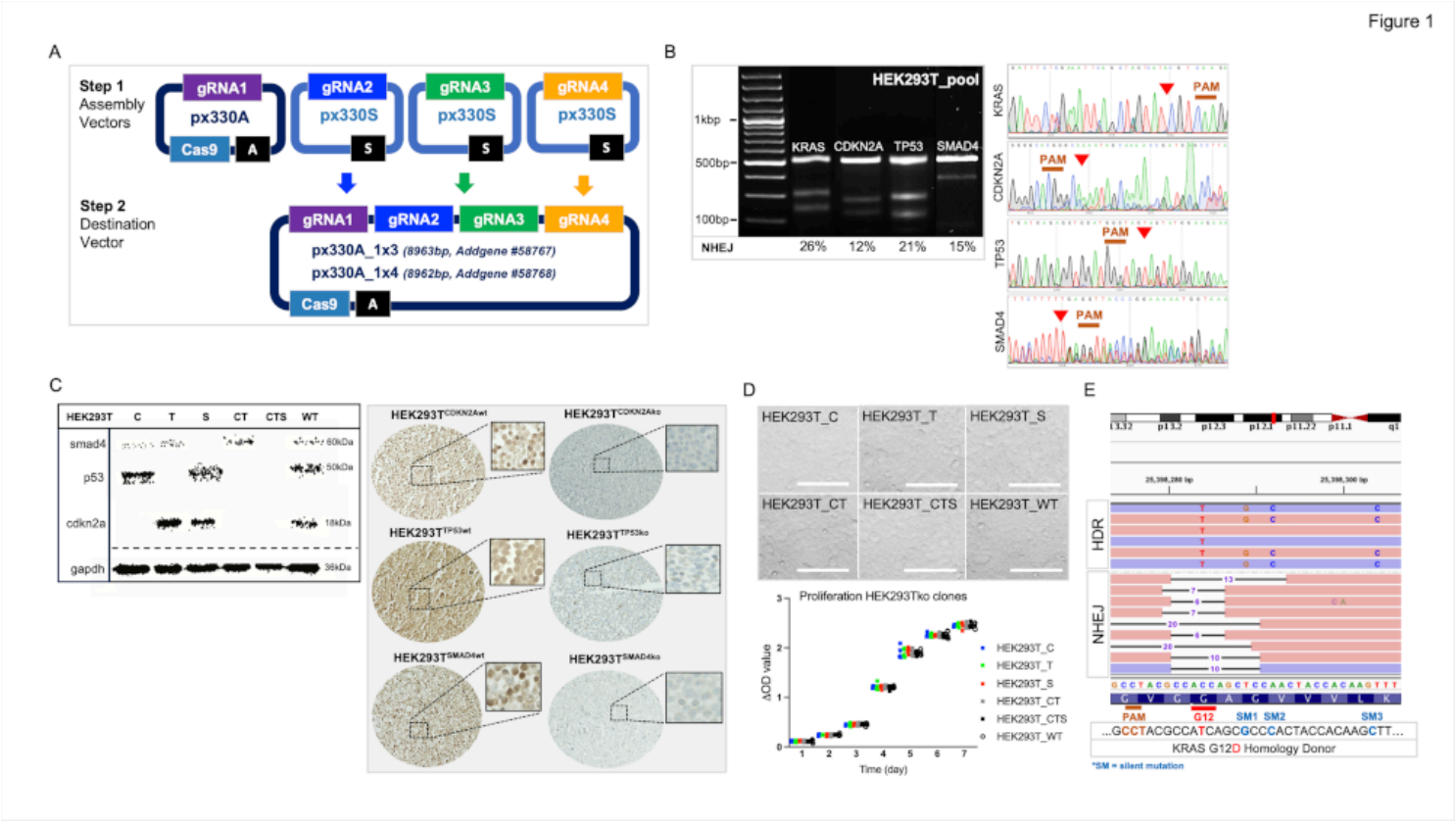

Figure 1

Effective driver gene editing via Golden Gate assembly for generation of multiplexed vectors.

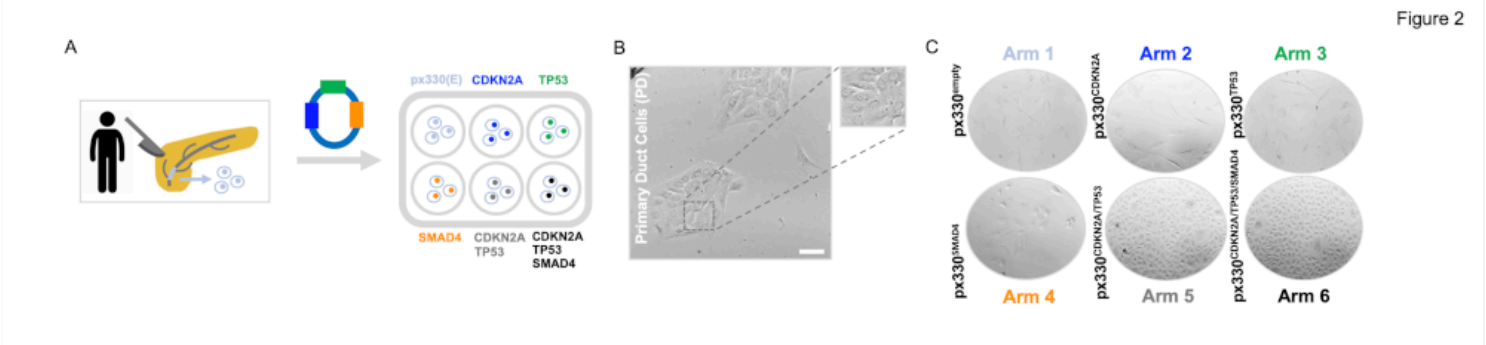

Figure 2

Natural selection of primary pancreatic ductal cells.

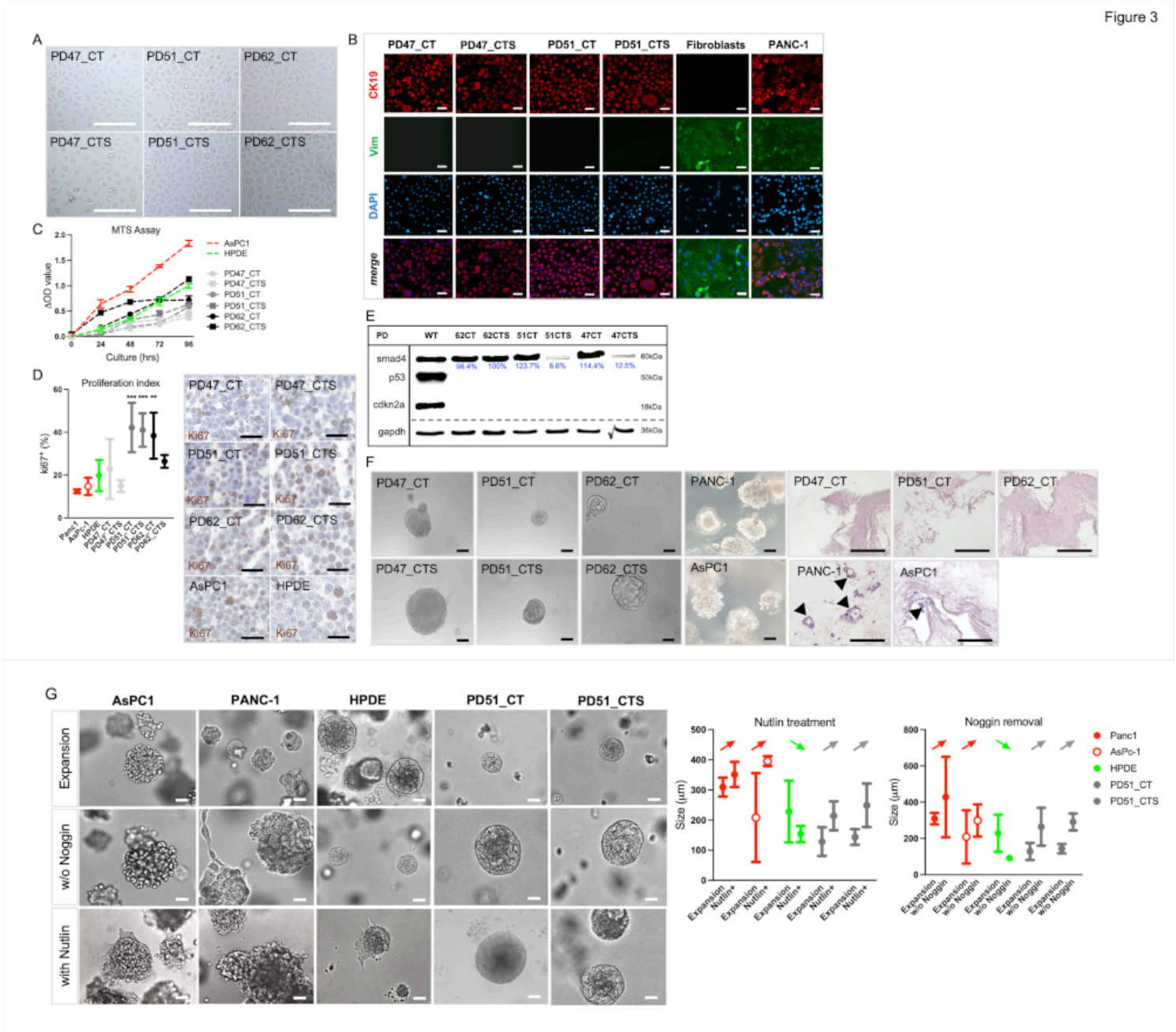

Figure 3

Characterization of immortalized primary duct cell lines.

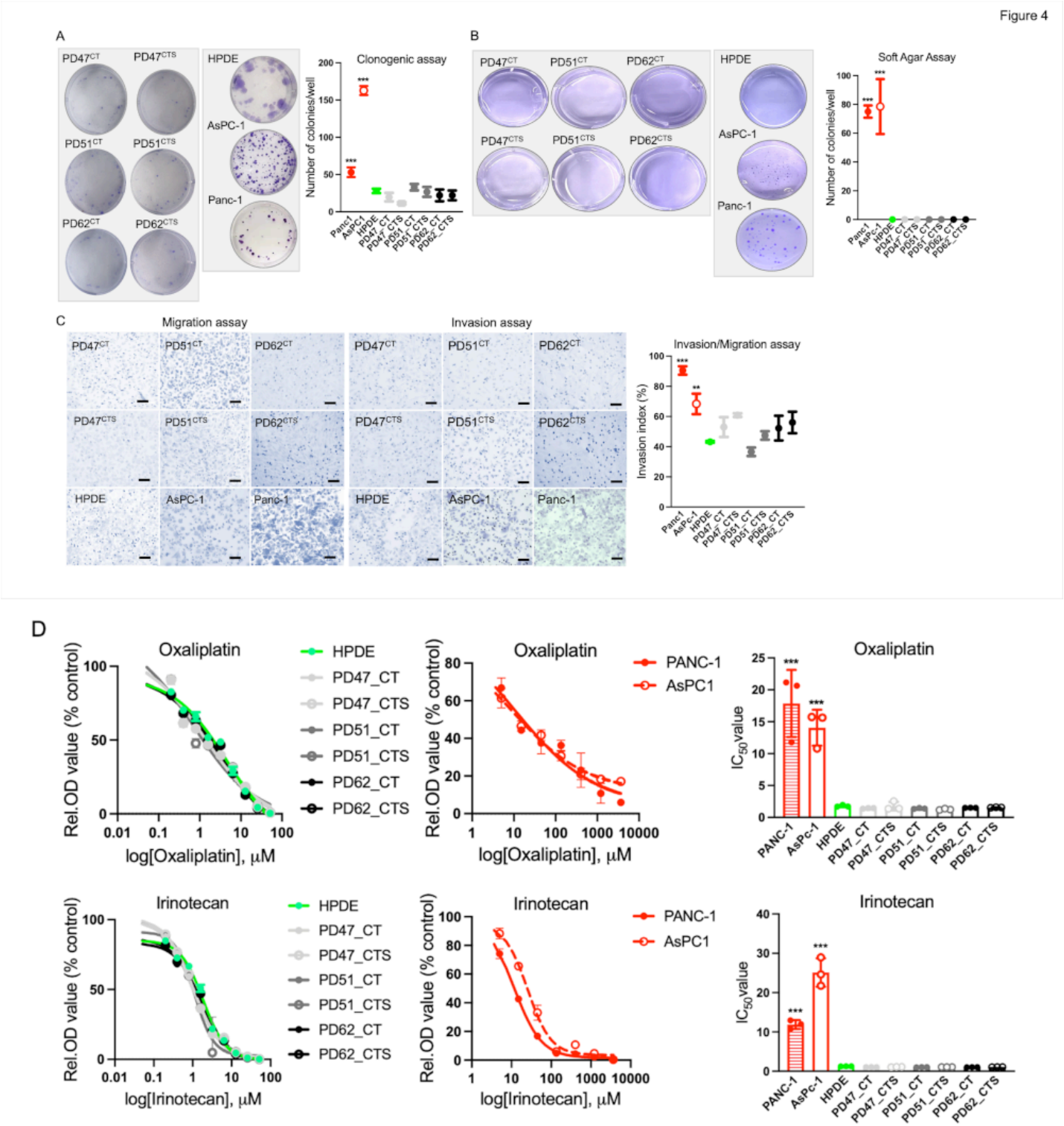

Figure 4

Tumorigenicity assessment of precursor cell lines.

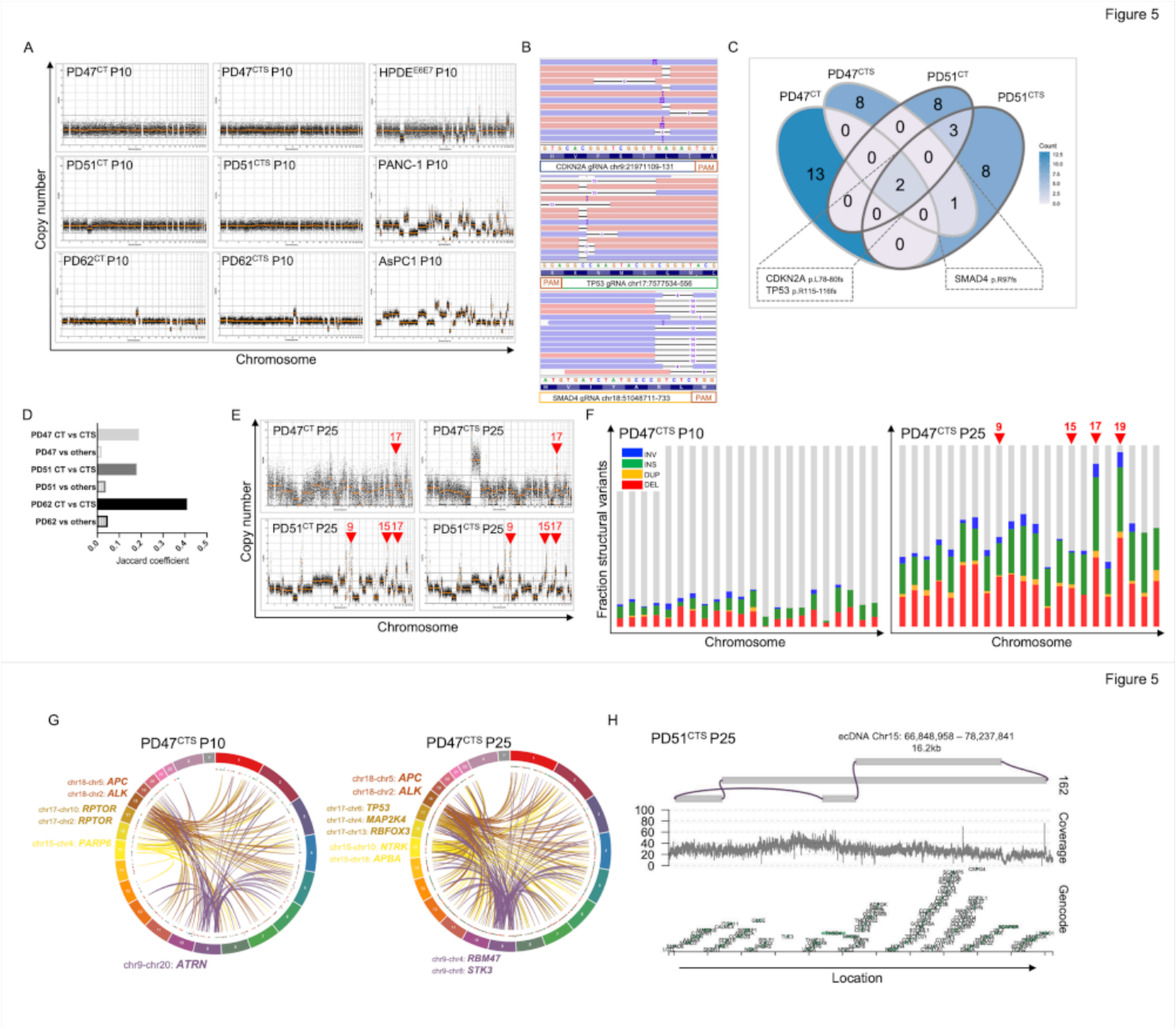

Figure 5

Genomic evolution following driver gene targeting.

Supplementary Files

This is a list of supplementary files associated with this preprint. Click to download.

- SUPPLEMENTARYFIGURESandTablesLegends.docx
- SupplTable2.pdf
- SupplTable4.pdf
- SupplTable3.pdf

- SupplTable6.pdf
- SupplTable7.pdf
- SupplTable5.pdf
- SupplFig.pdf
- SupplTable1.pdf
- AnnotatedSummaryoriginals.pdf
- TABLES.docx